Acta Materialia 111 (2016) 116–128

Contents lists available at ScienceDirect

Acta Materialia

journal homepage: www.elsevier.com/locate/actamat

Full length article

Crystal plasticity modeling of size effects in rolled multilayered Cu-Nb composites

N. Jia [a, *], D. Raabe [b, **], X. Zhao [a]

[a] Key Laboratory for Anisotropy and Texture of Materials (Ministry of Education), School of Material Science and Engineering, Northeastern University, Shenyang 110819, China
[b] Max-Planck-Institut für Eisenforschung, D-40237 Düsseldorf, Germany

ARTICLE INFO

Article history:
Received 8 January 2016
Received in revised form
25 February 2016
Accepted 19 March 2016

Keywords:
Multilayered composite
Shear band
Texture
Crystal plasticity finite element model

ABSTRACT

We present size-dependent crystal plasticity finite element simulations of the deformation microstructure, plastic flow and texture evolution in multilayered Cu-Nb composites during cold rolling. The model is based on a constitutive framework incorporating thermally activated dislocation slip, mechanical twinning and non-crystallographic shear banding. It also accounts for the dislocation density evolution and its dependence on initial grain size. By performing a series of quadricrystal simulations considering characteristic heterophase microstructures, the underlying micromechanics and texture of the composites are explored. Significant shear banding occurs in both phases, primarily determined by their initial orientations. For each phase, the activation of shear banding is also affected by the mechanical properties and orientations of the adjacent phase. For composites with an initial single layer thickness of 35 μm or 4 μm, the layer thickness reduction after rolling is non-uniform and the typical rolling textures for bulk pure metals develop in the respective phases. For the 75 nm initial single layer thickness composite, both phases are reduced uniformly in thickness and the initial orientations prevail. The predictions agree well with experimental observations in cold-rolled Cu-Nb thin films. The simulations reveal that for the composites with initial single layer thickness of micrometer scale, dislocation slip is the dominant deformation mechanism although shear banding increasingly carries the deformation at larger strains. For the samples with initial single layer thickness of a few tens of nanometers, shear banding and dislocation slip are the dominant mechanisms. This transition in deformation characteristics leads to different textures in micrometer- and nanometer-scaled multilayers.

1. Introduction

The mechanical behavior, radiation damage resistance and electrical properties of multilayered laminate-type composites, made up of alternating layers of two or more different metals, are of high basic and engineering interest [1–11]. Some of these composites reveal high strength and beneficial functional property, enabled by their small single layer thickness, individual phase properties and/or high heterophase interface density [12–15].

The numerous transmission electron microscopy (TEM) studies conducted on deformation of the composites synthesized by physical vapor deposition (PVD) [2–7] and accumulative roll bonding (ARB) [8–11] have shown that Hall-Petch type strain hardening governs the strength of micrometer-scaled multilayered composites [16]. For composites with single layer thickness of a few tens of nanometers, deformation is confined to Orowan-type dislocation glide within the individual layers [17,18]. When the layer thickness is reduced to a few nanometers, dislocation annihilation at the heterophase interfaces and single dislocation transmission across the interfaces prevails [3,19–21].

In addition, deformation of multilayered composites is characterized by trans-phase shear banding. Significant trans-phase deformation and interface instability were reported in a number of material systems, such as fcc/fcc (Cu-Au, Cu-Ag) [5,22,23], fcc/bcc (Cu-Nb, Cu-Cr) [24,25], fcc/hcp (Cu-Zr, Al-Mg) [7,10,22,26] and hcp/bcc (Zr/Nb) [27,28]. Shear bands are non-crystallographic band-like regions of concentrated plastic flow. Shear band deformation occurs in practically all bulk single-crystal and polycrystalline metals subjected to large deformations [29–33] and also in composites

* Corresponding author.
** Corresponding author.
E-mail addresses: jian@atm.neu.edu.cn (N. Jia), d.raabe@mpie.de (D. Raabe).

http://dx.doi.org/10.1016/j.actamat.2016.03.055
1359-6454/

with lamellar structures [5–7,10,22–26]. For multilayered composites one important type of microstructure associated with the development of shear bands, i.e. the heterogeneous deformation together with multiple curving and necking of the constituent layers, has been reported [5,6,22,23,27,34]. When well-developed shear bands run through heterophase interfaces, the relatively harder phase can be fragmented into diamond-shaped regions which are much less strained than the material inside the bands [22,34].

Crystallographic texture is an efficient indicator for revealing the underlying deformation mechanisms and it can help to guide bulk forming techniques for fabricating composite materials with beneficial texture and anisotropy. This close connection between deformation mechanisms and crystallographic texture motivate the study, placing specific attention on the texture development in deformed multilayers with different individual layer thicknesses. For instance, the rolling textures in PVD deposited Cu-Nb and also in metallurgically synthesized thin films with an initial Kurdjumov-Sachs (K-S) orientation relationship between the Cu and Nb layers have been studied in some detail [1,4,35]. After rolling to 50% thickness reduction, for micrometer-scaled single layer thickness laminates pronounced rolling textures were developed in the respective phases, while in nanolaminates the inherited K-S relationship between the phases was preserved. Studies on Cu-Nb multilayers with different single layer thicknesses during ARB also revealed that the textures developed in the two phases were distinctly different from classical rolling textures frequently observed in their single-phase counterparts [35–39]. Moreover, in a cold-rolled Cu-Ag eutectic nanocomposite [40], the measured texture components in the Cu phase were very different from the copper-type textures expected for rolled pure metals with medium or high stack fault energies [29]. The abnormal texture evolution in Cu, when embedded in a eutectic nanocomposite, was attributed to the influence of local constraints exerted from the phase boundary and the adjacent Ag phase, as revealed by both experiments and simulations [40,41]. Recently, the deviation of evolution of the deformation textures in nanolaminates from those observed in bulk pure metals was also reported in a Zr-Nb system [27,42]. These studies revealed that for smaller layer thickness the heterophase interfaces increasingly influence slip activity of the constituent phases, both, by constraints imposed by the grain boundary and by the kinetics of dislocation–interface interactions. Thus, in deformed multilayered composites specific texture components may evolve. Furthermore, our understanding of the dislocation slip kinetics in a multilayered heterophase structure, how the cross-phase shear banding accommodates the imposed boundary conditions among the metallic phases, as well as the effects of these mechanisms on texture evolution is still limited. Particularly, the micromechanical behaviors as a function of the initial layer thickness are still ambiguous.

In this work we use a crystal plasticity finite element (CPFE) model to study the inhomogeneity of deformation microstructure, plastic flow and texture evolution in multilayered Cu-Nb composites during cold rolling. The constitutive law considers crystallographic dislocation slip, deformation twining and non-crystallographic shear banding. The constitutive model is rendered size dependent since the dislocation density evolution depends on the initial grain size. Simulations are conducted for composites with different initial orientation combinations and single layer thicknesses. We focus on the micromechanical behavior of composites with initial single layer thickness above 75 nm. At this length scale the confined layer slip of single dislocations as well as dislocation transmission across interfaces can be neglected in Cu-Nb heterophase structures [3]. The simulations reveal that for a single layer thickness of a few tens of nanometers up to the micrometer length scale, the lattice reorientation of each individual layer is determined by its specific slip activity accompanied with the activation of shear bands.

2. Simulation procedures

We employ a CPFE model to study the mechanical behavior and texture evolution in deformed Cu-Nb heterophase composites. The model is based on a constitutive framework that incorporates shear banding as a separate non-crystallographic deformation mechanism in conjunction with dislocation slip and mechanical twinning [43]. A summary of the main constitutive formulations is given below.

2.1. Crystal plasticity based flow rule

We use the finite strain kinematic framework in which the deformation gradient, $\mathbf{F}$, is multiplicatively decomposed according to:

$$\mathbf{F} = \mathbf{F}^{e}\mathbf{F}^{p} \tag{1}$$

where $\mathbf{F}^{e}$ is the elastic part comprising the stretch, $\mathbf{U}^{e}$, and the lattice rotation, $\mathbf{R}^{e}$; $\mathbf{F}^{p}$ is the plastic part of the deformation gradient. The initial plastic deformation gradient $\mathbf{F}_{\mathbf{0}}^{p}$ is set to the inverse of the local crystal orientation, $\mathbf{T}_{0}^{-1}$, and evolves at a rate governed by the plastic velocity gradient $\mathbf{L}^{p}$:

$$\dot{\mathbf{F}}^{\mathbf{p}} = \mathbf{L}^{\mathbf{p}}\mathbf{F}^{\mathbf{p}} \tag{2}$$

The evolution of the crystal orientation with strain then follows the polar decomposition $\mathbf{F}^{e} = \mathbf{R}^{e}\,\mathbf{U}^{e}$ as $\mathbf{T} = \mathbf{R}^{e}$. Inspired by Kalidindi [44] and Steinmetz [45], the plastic velocity gradient, $\mathbf{L}^{p}$, has contributions from dislocation slip systems, twinning systems, and shear banding:

$$\mathbf{L}^{p} = \sum_{\alpha=1}^{Nslip} \dot{\gamma}^{\alpha}\mathbf{m}^{\alpha}\otimes\mathbf{n}^{\alpha} + \sum_{\beta=1}^{Ntwin} \dot{\gamma}^{\beta}\mathbf{m}_{twin}^{\beta}\otimes\mathbf{n}_{twin}^{\beta} + \sum_{\chi=1}^{Nsb} \dot{\gamma}^{\chi}\mathbf{m}_{sb}^{\chi}\otimes\mathbf{n}_{sb}^{\chi} \tag{3}$$

The vectors $\mathbf{m}$ and $\mathbf{n}$ denote the directions and plane normals of the deformation systems on which shear occurs at a rate $\dot{\gamma}$. However, different from Ref. [44], we assume that twins can be further sheared by dislocation slip in a manner compatible to the surrounding matrix, and evolution of slip resistance within the twins is identical to that outside the twinned region. For this scenario the volume fraction of the non-twinned crystal portions in the contribution of dislocation slip can be omitted in Eq. (3).

2.2. Constitutive formulations for dislocation slip, twinning and shear banding

For both phases each slip system follows an individual dislocation density evolution that depends on the initial grain size. This form renders the constitutive model size dependent. Following the work of Blum and Eisenlohr [46], the evolution of dislocation densities is related to dislocation multiplication, dipole formation and dislocation annihilation. The flow rule describes thermally activated dislocation motion through forest dislocations. The shear rate of the slip system α is:

$$\dot{\gamma}^{\alpha} = \rho_{sgl}^{\alpha} b v_{0} exp\left[\left(-\frac{Q_{0}}{k_{B}T}\left(1-\frac{|\tau^{\alpha}|}{\hat{\tau}^{\alpha}}\right)^{p}\right)^{q}\right]\mathrm{sign}(\tau^{\alpha}) \tag{4}$$

where τ^{α} is the current resolved shear stress; $\widehat{\tau}^{\alpha}$ is the slip resistance governed by the dislocation population; $\rho^{\alpha}_{\mathrm{sgl}}$ is the density of single dislocations; b is the length of the Burgers vector; v_0 is the dislocation velocity of the slip system when subjected to a stress equal to the slip resistance $\widehat{\tau}^{\alpha}$; Q_0 is the activation energy for dislocation slip; k_{B} and T denote the Boltzmann constant and temperature, respectively; p and q are numerical parameters to adjust the obstacle profile [47]. Considering that each dislocation segment is either a single dislocation or part of a stable dipole [46], the slip resistance $\widehat{\tau}^{\alpha}$ depends on the dislocation densities as

$$\widehat{\tau}^{\alpha} = \tau_0 + Gb\left(\sum_{\alpha'=1}^{N\mathrm{slip}} \xi_{\alpha\alpha'}\left(\rho^{\alpha'}_{\mathrm{sgl}} + \rho^{\alpha'}_{\mathrm{dip}}\right)\right)^{1/2} \tag{5}$$

with τ_0 the athermal glide resistance, G the shear modulus, $\rho^{\alpha'}_{\mathrm{dip}}$ the dipolar dislocation density, and $\xi_{\alpha\alpha'}$ characterizes the interaction strength between different slip systems α and α'.τ_0 represents the slip resistance to the propagation of dislocation apart from dislocation–dislocation interactions [28]. Thus, it does not evolve with strain and is given by a sum of the lattice friction stress $\tau_{0,\mathrm{f}}$ and the grain-size dependent Hall-Petch contribution:

$$\tau_0 = \tau_{0,\mathrm{f}} + k_{\mathrm{y}} {d_{\mathrm{grain}}}^{-1/2} \tag{6}$$

where k_{y} is the Hall-Petch slope (also referred to as grain boundary resistance), and d_{grain} is the initial grain size. Following Ma and Roters [48], the dislocation density on any particular system β can be projected with respect to system α into a corresponding forest density. Then, by summation of the contribution of each slip system β the overall forest dislocation density on system α amounts to

$$\rho^{\alpha} = \sum_{\beta=1}^{N\mathrm{slip}} \left[\left(\rho^{\beta}_{\mathrm{sgl}} + \rho^{\beta}_{\mathrm{dip}}\right)\left|\mathbf{n}^{\alpha}\cdot\mathbf{t}^{\beta}\right|\right] \tag{7}$$

with vector $\mathbf{t}$ the tangent vector (cross product) of the slip plane normal and the slip direction, i.e. $\mathbf{t} = \mathbf{m} \times \mathbf{n}$. The rate equation of the dislocation multiplication is in the form $d\rho = \frac{|d\gamma^{\alpha}|}{b\lambda^{\alpha}}$, where λ^{α} is the effective spacing for dislocation slip between obstacles. Specifically, to capture the size-dependence of the micromechanical response, the mean free path of the dislocations is affected by grain size according to

$$\frac{1}{\lambda^{\alpha}} = \frac{1}{d_{\mathrm{grain}}} + \frac{\sqrt{\rho^{\alpha}}}{c} \tag{8}$$

where c is a constant controlling the dislocation mean free path. The model also considers athermally activated annihilation of dipoles [47], which leads to a decrease in the overall dislocation density. Out of all dipoles formed by glide those with a glide plane separation below $\widehat{d}^{\alpha}$ annihilate instantaneously:

$$\mathrm{d}\rho^{\alpha}_{\mathrm{sgl}} = -\frac{2\widehat{d}^{\alpha}}{b}\rho^{\alpha}_{\mathrm{sgl}}|\mathrm{d}\gamma^{\alpha}| \tag{9}$$

A second athermal annihilation opportunity is due to single dislocations recombining with a compatible constituent from an already existing dipole, which is expressed as

$$\mathrm{d}\rho^{\alpha}_{\mathrm{sgl}} = -\frac{2\widehat{d}^{\alpha}}{b}\rho^{\alpha}_{\mathrm{dip}}|\mathrm{d}\gamma^{\alpha}| \tag{10}$$

Based on the twin nucleation scheme proposed by Mahajan et al. [49], it is assumed that the critical twin nucleation event consists in the correlated bow-out of three partial dislocations between pinning points separated by a microscopic length scale L_0 [45]. Then, the critical stress for twin formation is calculated as

$$\widehat{\tau}_{\mathrm{twin}} = \frac{\gamma_{\mathrm{sf}}}{3b_{\mathrm{twin}}} + \frac{3Gb_{\mathrm{twin}}}{L_0} \tag{11}$$

where b_{twin} is the Burgers vector of the moving partials and γ_{sf} is the stacking fault energy of the material. With the presence of twins, the effective spacing for dislocation slip between obstacles λ^{α} has to include twin boundaries as additional obstacles to dislocation motion. Correspondingly, the mean free path of the dislocations, calculated as harmonic mean in Eq. (8), is modified as

$$\frac{1}{\lambda^{\alpha}} = \frac{1}{d_{\mathrm{grain}}} + \frac{\sqrt{\rho^{\alpha}}}{c} + \sum_{\beta=1}^{N\mathrm{twin}} \xi_{\alpha\beta}\frac{1}{d^{\beta}_{\mathrm{twin}}} \tag{12}$$

where $\xi_{\alpha\beta}$ is the slip–twin interaction parameter characterizing the interaction between slip system α and twin system β and d_{twin} is the twin size that evolves with the twin volume fraction. As twinning is not the dominant deformation mechanism in either phase of the Cu-Nb composite, details of the twin model already described in Refs. [45,47] are omitted here.

For shear banding as a third deformation mechanism, we refer to the model originally developed by Anand et al. [50] for amorphous metallic materials. In this model deformation occurs on specific non-crystallographic shear banding systems that are defined relative to the three (variable) principal directions of the second Piola–Kirchhoff stress $\mathbf{T}^{\mathrm{e}}$ (conjugated to the elastic Green–Lagrange strain). The spectral decomposition of the Piola–Kirchhoff stress $\mathbf{T}^{\mathrm{e}}$ is:

$$\mathbf{T}^{\mathrm{e}} = \sum_{i=1}^{3} \sigma_i\, \widehat{\mathbf{e}}_i \otimes \widehat{\mathbf{e}}_i \tag{13}$$

where σ_i are the principal stresses and $\widehat{\mathbf{e}}_i$ the orthonormal principal directions of $\mathbf{T}^{\mathrm{e}}$. Plastic flow due to shear banding is considered on six potential systems in the planes constructed by the three principal stress directions. In each $(\widehat{\mathbf{e}}_i - \widehat{\mathbf{e}}_j)$-plane, the two potential shear band systems are specified by a direction $\mathbf{m}$, and a plane normal $\mathbf{n}$:

$$\mathbf{m}^{(1)} = cos(\pi/4)\widehat{\mathbf{e}}_i + sin(\pi/4)\widehat{\mathbf{e}}_j,\ \mathbf{n}^{(1)} = \sin(\pi/4)\widehat{\mathbf{e}}_i - \cos(\pi/4)\widehat{\mathbf{e}}_j$$

$$\mathbf{m}^{(2)} = \cos(\pi/4)\widehat{\mathbf{e}}_i - \sin(\pi/4)\widehat{\mathbf{e}}_j,\ \mathbf{n}^{(2)} = \sin(\pi/4)\widehat{\mathbf{e}}_i + \cos(\pi/4)\widehat{\mathbf{e}}_j \tag{14}$$

where the indices i and j range from 1 to 3 with $i \neq j$. The superscripts on $\mathbf{m}$ and $\mathbf{n}$ denote the identifier of each system. The governing condition for the activation of shear bands is realized by the attainment of a critical resolved stress criterion, i.e. a resistance to shear banding. The shear rate $\dot{\gamma}^{\chi}$ of the shear band system χ is formulated in analogy to that used for the slip systems [43]:

$$\dot{\gamma}^{\chi} = \dot{\gamma}^{\chi}_0 exp\left[\left(-\frac{Q_0}{k_{\mathrm{B}}T}\left(1 - \frac{|\tau^{\chi}|}{\widehat{\tau}_{\mathrm{sb}}}\right)^{p}\right)^{q}\right] sign(\tau^{\chi}) \tag{15}$$

where $\dot{\gamma}^{\chi}_0$ is a reference shear rate, τ^{χ} is the resolved stress on system χ, and $\widehat{\tau}_{\mathrm{sb}}$ is the constant threshold stress for shear banding. The parameters p, q and Q_0 are same as that used for dislocation slip.

The constitutive parameters of the individual Cu and Nb phases are determined by fitting the macroscopic stress vs. strain curves

obtained from uniaxial tensile tests for each of the pure metals with an average initial grain size of 35 μm [51,52], as listed in the Supplemental material. For the fcc Cu phase, 12 {111}<110> dislocation slip systems and 12 {111}<112> twinning systems are considered. For the bcc Nb phase, two types of slip systems with a common <111> direction, i.e. {110}<111> and {112}<111>, are considered [36,53,54]. As prior study on rolled Cu-Nb bimetallic multilayers did not indicate twinning in Nb even at the finest nanoscale thicknesses [55], we assume here that twinning does not occur in the Nb phase.

To also simulate co-deformation of Cu-Nb quadricrystals with different initial single layer thickness, considering that the activation of both, slip and shear band deformation are related to the material's strength, the critical resolved shear stress for activating dislocation slip and shear banding varies among the different quadricrystal combinations. Following the steps below the relevant material parameters are determined. First, by fitting the flow stress vs. layer thickness curve of the Cu-Nb multilayers measured by nanoindentation [3], the $\tau_{0,f}$ (lattice friction stress) and k_y (the Hall-Petch slope) values of the respective phases are determined. The deduced yield stresses of the Cu-Nb multilayers fit the Hall-Petch law that is attributed to dislocation pile-ups against phase boundaries when the individual layer thickness is above 75 nm. As mentioned above, for samples with initial single layer thickness of 35 μm the threshold stress of shear banding in respective phases has been obtained by fitting the tensile curves of each bulk pure metal. Then, the $\hat{\tau}_{sb}$ values of the 4 μm and 75 nm layer thickness samples are subsequently fixed by multiplying their respective τ_0 with a scale-up factor,

$$\hat{\tau}_{sb}^{(4\mu m)} = \tau_0^{(4\mu m)} \frac{\hat{\tau}_{sb}^{(35\mu m)}}{\tau_0^{(35\mu m)}} \text{ and } \hat{\tau}_{sb}^{(75nm)} = \tau_0^{(75nm)} \frac{\hat{\tau}_{sb}^{(35\mu m)}}{\tau_0^{(35\mu m)}} \quad (16)$$

where $\tau_0^{(35\mu m)}$ and $\hat{\tau}_{sb}^{(35\mu m)}$ are the athermal slip resistance and the threshold stress to initiate shear banding for the 35 μm layer thickness sample, respectively. All other constitutive parameters are identical for the differently layer-sized samples.

2.3. Model set-up and simulation runs

Based on the constitutive laws outlined above, the CPFE simulations of the Cu-Nb heterophase composites during cold rolling were carried out using the finite element solver MSC.Marc2013 in conjunction with an open source user defined material subroutine coded in the free DAMASK simulation package [55–57]. The current study firstly focuses on the simulation of Cu plus Nb multilayered composites (quadricrystals) with specific initial orientation combinations. Then, for the study of micromechanical behavior in Cu-Nb composites as a function of initial single layer thickness, deformation of quadricrystals with individual layer thickness ranging from 35 μm to 75 nm is simulated. For both parts of the study, detailed results on local orientation distributions, shear band topology and the governing micromechanisms are presented.

For quadricrystal simulations throughout this paper, the modeled region is a portion of a bulk material with a thickness-to-length ratio (H_0:L_0) of 2.0 in the undeformed state, as shown in Fig. 1. The Cu and Nb crystals with the same thickness are mutually stacked so that the overall composition amounts to a Cu-Nb volume fraction of 50:50. Plane strain compression is used as an approximation of the deformation in the mid-thickness layers of an actual rolling process [58]. The elongation direction (ED), normal direction (ND), and transverse direction (TD) are set to coincide with a Cartesian coordinate system, *X*, *Y*, and *Z*, respectively. A prescribed displacement corresponding to the thickness reduction is applied

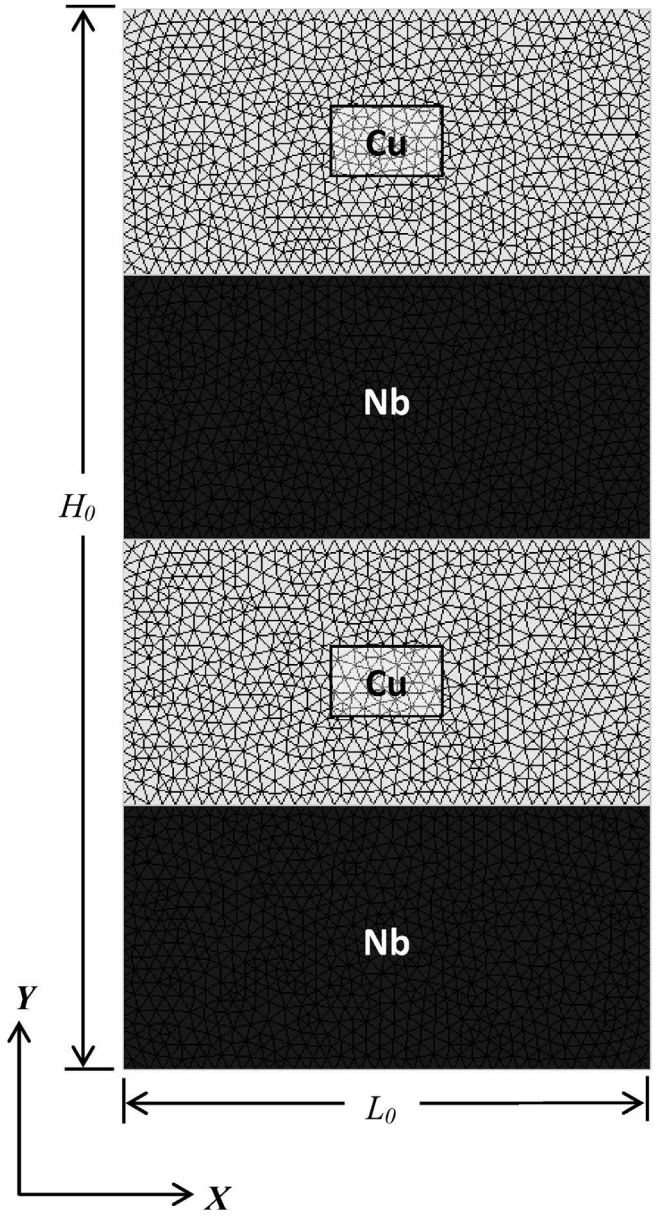

Fig. 1. Schematic of a two-dimensional heterophase Cu-Nb quadricrystal model consisting of triangular elements (Cu phase in light gray and Nb phase in dark gray). To simulate plane strain compression, a prescribed displacement corresponding to the thickness reduction is applied to the top edge. The left and bottom edges are constrained from moving in the *X* and *Y* directions, respectively. The right edge is permitted to move in the *X* direction.

to the top edge with a strain rate of 10^{-3} s^{-1}. The right edge is free to move in the *X* (forward) direction. The left and bottom edges are constrained from moving in the *X* and *Y* directions, respectively. Multi-point constraints are applied to maintain the right edge straight during deformation. Simulations on two Cu-Nb lamellar configurations with specific initial orientation combinations, i.e. Cu (Copper orientation, $(1\,1\,2)[1\,1\,\bar{1}]$) plus Nb (Brass-R orientation and Cu (KS-fcc orientation, $(1\,1\,1)[1\,\bar{1}\,0]$) plus Nb (KS-bcc orientation, $(1\,1\,0)[1\,\bar{1}\,1]$) are performed (see Table 1). The rationale behind this selection is as follows: Copper and Brass-R represent the texture components that promote shear banding in fcc and bcc materials, respectively [59]. Moreover, many experimental data sets on plane strain compressed Cu-Nb multilayers with heterophase interfaces locally satisfying the K-S orientation relations (ND//$<111>_{Cu}$//

Table 1
Miller indices and Euler angles of the ideal texture orientations in fcc and bcc metals.

Component	Indices {*h k l*}<*u v w*>	Bunge (φ_1, Φ and φ_2)
Copper	{112}<111>	90°, 35°, 45°
KS-fcc	{111}<110>	0°, 55°, 45°
Goss	{011}<100>	0°, 45°, 0°
Brass-R	{111}<112>	90°, 55°, 45°
KS-bcc	{110}<111>	35°, 90°, 45°
Rotated-cube	{001}<110>	0°, 0°, 45°

$<110>_{Nb}$ and ED//$<110>_{Cu}$//$<111>_{Nb}$) are available [1,2,4,24,37]. This motivates the choice of KS-fcc and KS-bcc as the initial crystallographic orientations for Cu and Nb crystals, respectively. Another reason is that the two composites with the selected initial orientations exhibit different plastic stability as will be shown in Section 3. In this part of the work, an average grain size of 35 μm is assumed for all the constituent phases in the quadricrystal simulations. Deformation of Cu and Nb single crystals with the initial orientations as mentioned above is also modeled. The same geometry and boundary conditions as those used for the quadricrystals are applied to the single crystal models.

3. Simulation results

3.1. Mechanical response of single crystals

Fig. 2a and b show the equivalent true stress–strain curves of the Cu and Nb single crystals with the above-mentioned initial orientations, respectively. The mechanical behavior of the orientations that do not favor the initiation of shear banding in the respective phases, i.e. Goss orientation ((0 1 1)[1 0 0]) in Cu and Rotated-cube orientation ((0 0 1)[1 $\bar{1}$ 0]) in Nb (Table 1), are also shown for comparison. In Fig. 2, the relative shear contributions of the competing deformation systems (dislocation slip, mechanical twinning and shear banding) as a function of the equivalent true strain are also given. The individual contributions are given as summations over the absolute values of the shear rates on the different systems for each type of mechanism, and then normalized by the overall shear at each deformation step. The deformation stage where the contribution stemming from shear banding amounts to a strain of 0.1 is marked by the symbol '○'. For Cu crystals with initial Copper and KS-fcc orientations, the model predicts that a strain of 0.1 from shear banding occurs at a stress of 280 and 262 MPa, respectively. This result reveals that when the stress reaches those values for the respective single crystals, shear banding sets in as a significant deformation mechanism. With further deformation, as only minor twinning deformation is activated, shear banding and dislocation slip are the dominant mechanisms. The initially Goss-oriented Cu crystal shows zero shear contribution from shear banding and twinning during plastic straining. The predictions for the Cu single crystals generally agree with the previous study on the orientation-dependent shear banding behavior of an aluminum alloy [60]. For the initially Brass-R and KS-bcc oriented Nb single crystals, the simulation predicts that the increase in the shear contributed by shear banding occurs at a stress of 320 and 150 MPa, respectively. In addition, further

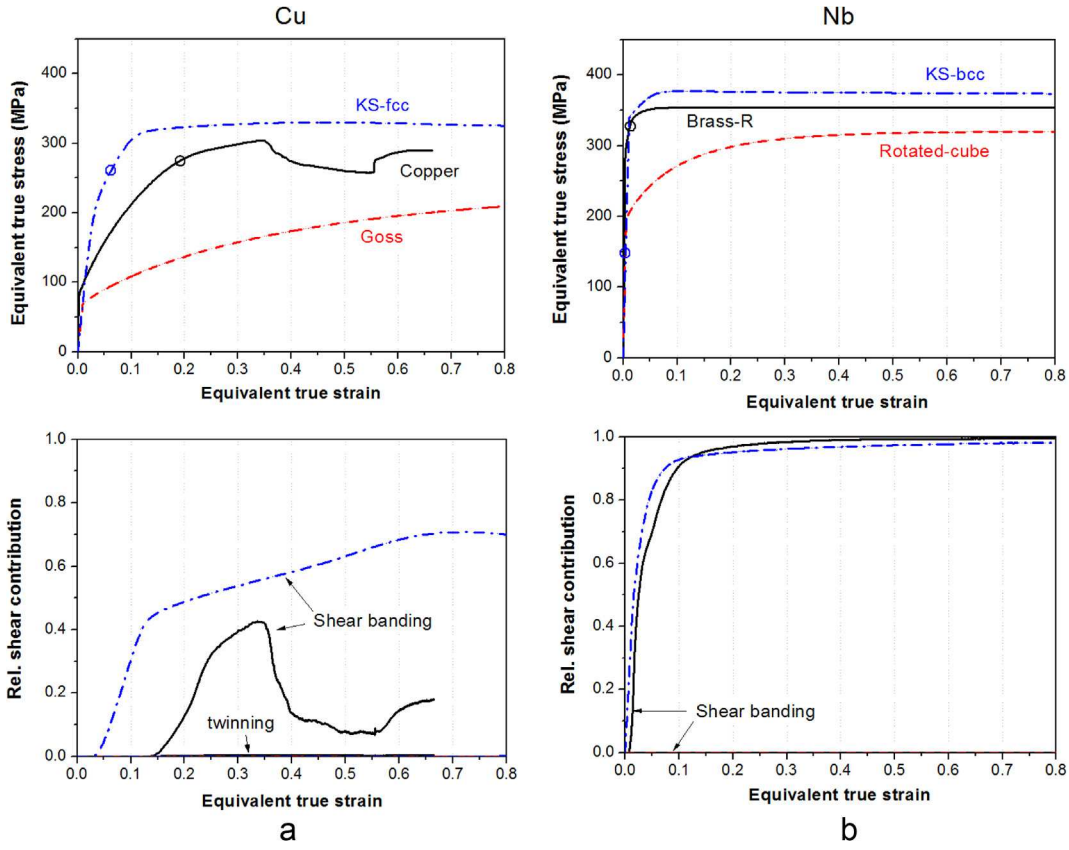

Fig. 2. Predicted stress–strain curves and relative shear contributed by the different deformation mechanisms (twinning and non-crystallographic shear banding) as a function of the equivalent true strain for (a) Cu and (b) Nb single crystals with different initial crystallographic orientations during plane strain compression. As the total shear contribution from dislocation slip, twinning and shear banding for each textured material is 1.0, the relative shear from dislocation slip is not shown. The corresponding initial orientations are explained in the text.

deformation proceeds mainly via shear banding rather than via dislocation slip. These results show that in these materials shear banding is readily activated. For the initially Rotated-cube textured Nb material, shear banding does not occur within the entire deformation range.

3.2. Mechanical response of quadricrystals with specific initial orientation combinations

The simulated results for the Cu-Nb quadricrystals with different orientation combinations are presented in terms of the distribution of grain rotation angle, sum of shear rates on the shear band systems, equivalent logarithmic strain and equivalent Cauchy stress at 50% thickness reduction, as shown in Fig. 3. The rotation angle is defined as the misorientation angle relative to the initial orientation of each crystal.

For the Cu (Copper orientation) plus Nb (Brass-R orientation) quadricrystal (Fig. 3a), a significant localization of both strain and shear banding appears inside the Cu and Nb layers. The localized zones are connected with each other across the heterophase interfaces, indicating that the initiation of shear banding in Cu (adjacent to Nb layer) is triggered by stress concentration at the phase boundaries. The difference in stress between the Cu and Nb phases is also clearly identified. This leads to strain localization of multiple directions in both phases as well as severe curvature of the phase boundaries, which agrees with experimental observations of such cold-rolled composites that show significant inclination of phase boundaries with respect to ED [5,22–25,61]. In the current configuration, both phases have initial orientations that promote shear banding. Then, when local stresses reach a critical value the activation of shear bands can be triggered in this phase. It should be noticed that the finite element meshing gets highly distorted due to the strain localization in the shear banding zones. In addition, a larger lattice rotation above 20° is localized inside the Cu layers, and a larger rotation above 10° appears in the Nb layers. The localized area of the Nb layers is connected to the adjacent strain localization zone of the Cu regions, and the material points with larger grain rotations correspond to zones with higher stresses. In both phases, the occurrence of localized rotation coincides with the initiation of shear banding. Actually, at around 20% thickness

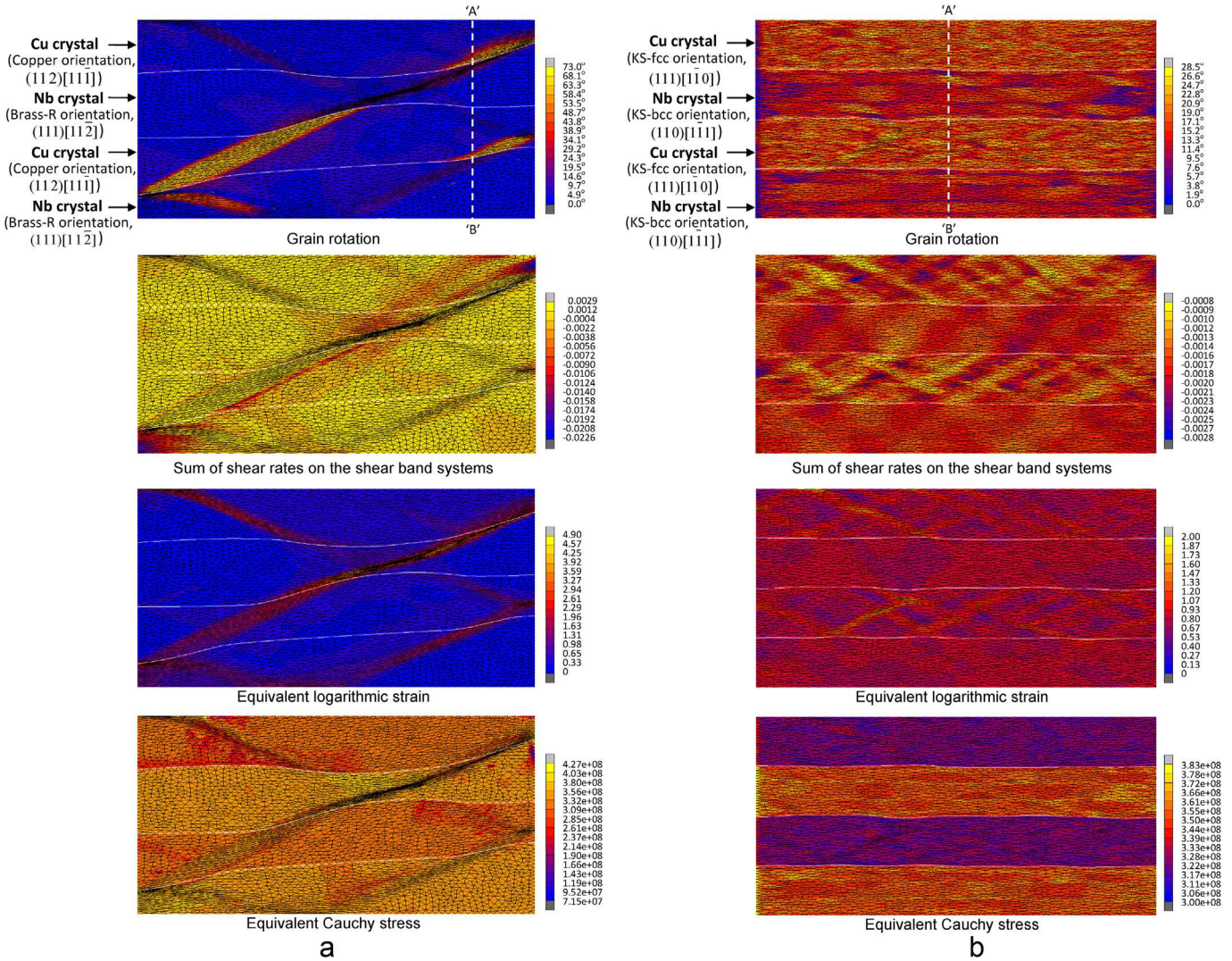

Fig. 3. Predicted distributions of grain rotation angle, sum of shear rates on the shear band systems, equivalent logarithmic strain and equivalent Cauchy stress for Cu-Nb quadricrystals with different initial orientations at 50% thickness reduction: (a) Cu (Copper orientation, (1 1 2)[1 1 $\bar{1}$]) plus Nb (Brass-R orientation, (1 1 1)[1 1 $\bar{2}$]) heterophase quadricrystal and (b) Cu (KS-fcc orientation, (1 1 1)[1 $\bar{1}$ 0]) plus Nb (KS-bcc orientation, (1 1 0)[1 $\bar{1}$ 1]) heterophase quadricrystal. In the quadricrystal models, the initial grain size that corresponds to the initial layer thickness is 35 μm. The white lines indicate interfaces between abutting crystals.

reduction the activation of shear banding occurs in regions of both phases where the stress reaches the respective critical values identified in Fig. 1. With increasing deformation the stress field inside the sample becomes more homogeneously distributed. Correspondingly, the shear rates of the shear bands decrease within the bands. Our previous simulations on cold-rolled fcc single crystals have shown that the occurrence of shear bands corresponds to a rotation of the in-band region around TD [62]. This kinematic effect facilitates strain accommodation by homogeneous slip along the shear plane. Consequently, the area outside the bands is gradually incorporated into the bands with ongoing loading. This effect becomes visible in the form of shear band thickening both, in experiment [31,32] and modeling [62].

The simulation results for the Cu (KS-fcc orientation) plus Nb (KS-bcc orientation) quadricrystal is shown in Fig. 3b. Generally uniform reduction in layer thickness with only minor curvature of the phase boundaries is observed. Compared to the Cu (Copper orientation) plus Nb (Brass-R orientation) quadricrystal, the equivalent logarithmic strain and equivalent Cauchy stress are more homogeneously distributed in each individual phase. Moreover, in both phases the shear rate of shear banding is smaller, even though the initial orientations of the respective phases also show a large tendency to initiate shear banding (Fig. 2). This is due to the fact that the difference in stress between the constituent metals is small, which leads to a homogeneous plastic deformation of the entire sample. In this case, the maximum grain rotation is less than 28.5° and 5° for the Cu and Nb phases, respectively.

3.3. Mechanical response of quadricrystals with different initial single layer thicknesses

According to the above simulations, the deformed Cu (Copper orientation) plus Nb (Brass-R orientation) quadricrystal and Cu (KS-fcc orientation) plus Nb (KS-bcc orientation) quadricrystal with a 35 μm initial single layer thickness exhibit different plastic stability, i.e. the difference in terms of layer topology, distribution of stress, strain and shear banding (Fig. 3a and b). In this section we explore the influence of the initial single layer thickness on the mechanical response as well as on the orientation distribution of the multilayered structures. For the sake of brevity, we only present the results of equivalent logarithmic strain and equivalent Cauchy stress for composites with initial individual layer thicknesses of 4 μm and 75 nm, respectively, after 50% deformation. The distributions of grain rotation angle and sum of shear rates on the shear band systems are included in Supplementary material (Fig. S2). For the Cu (Copper orientation) plus Nb (Brass-R orientation) quadricrystal with an initial single layer thickness of 4 μm (Fig. 4a), strain localization is at the same level as for the corresponding quadricrystal with an initial single layer thickness of 35 μm (Fig. 3a), indicative of the incompatibility of deformation between the Cu and Nb phases. An inhomogeneous distribution of stress within the microstructure is also observed. In the respective phases, the shear band and grain rotation angle patterns are consistent with the stress patterns. The quadricrystal with 75 nm initial single layer thickness shows a much less significant strain accumulation in both phases and no inclination of the phase boundaries with respect to ED can be identified (Fig. 4b). In this sample, despite the equivalent Cauchy stresses in both phases are much higher than that of the quadricrystals with an initial single layer thickness of 35 μm or 4 μm, the shear band systems have been homogeneously activated at the constituent material points. This indicates the increasing compatibility of deformation between the phases. In the nanometer-scaled sample, the maximum grain rotation is less than 3° in both Cu and Nb layers.

The simulation results for the Cu (KS-fcc orientation) plus Nb (KS-bcc orientation) quadricrystals with initial single layer thicknesses of 4 μm and 75 nm are shown in Fig. 4c and d, respectively. In both samples the Cu and Nb layers are reduced in thickness uniformly. The strain, stress and shear rates of the shear bands are homogeneously distributed in each individual phase. This means that despite their very different strengths, the two alternating phases respond identically to the external loading with a joint uniform reduction in layer thickness. However, the maximum grain rotation is different between the samples. In the 4 μm layer thickness quadricrystal the grain rotation is similar to that of the sample with an initial single layer thickness of 35 μm, showing maximum rotation angles of 28.5° and 5° in Cu and Nb, respectively. However, in the 75 nm layer thickness quadricrystal, only very minor rotations occur in both phases. Specifically, the K-S orientation relation is preserved.

4. Discussion

4.1. Lattice reorientation and micromechanics in heterophase quadricrystals

For exploring lattice reorientations and micromechanics in the heterophase quadricrystals with specific initial orientations, the predicted texture and strain patterns along the line AB, parallel to ND, are traced for the quadricrystals with initial layer thickness of 35 μm. As indicated in Fig. 3, in each sample the line passes through zones with significant strain localization and severe phase boundary curvature. The grain rotation angle and equivalent true strain for the quadricrystals at 50% thickness reduction is plotted as a function of the 40 evaluated points from 'A' to 'B', as shown in Fig. 5. For each plot, the {111} and {110} pole figures of the most heavily rotated material points in the Cu and Nb layers of the deformed quadricrystals are given in the Supplementary material. To identify the effects of the neighboring phases (or heterophase interfaces), the new orientation corresponding to the maximum rotation angle of the single crystals under the same deformation is also shown (Fig. S3, Supplementary material).

For the Cu (Copper orientation) plus Nb (Brass-R orientation) quadricrystal, significant rotation of the Cu layers within a range of 45–60° is found close to the two phase boundaries, i.e. between the upper Cu and Nb layers and between the lower Cu and Nb layers (Fig. 5a). This corresponds to a rotation of the original Copper orientation about TD towards $(4\,4\,1)[\bar{1}\,\bar{1}\,8]$ which is close to the Goss component. The rotation is typically observed experimentally in Copper-oriented Cu single crystals deformed at 77 K and in low stacking fault energy fcc single crystals such as Cu-Al and pure Ag deformed at room temperature [30,31]. Also, regions with large rotations exhibit some shear banding and accumulated strain, yet, the reverse may not generally hold. This means that strain localization does not necessarily occur in regions of large rotation. In the interior of the upper Cu layer a true strain up to ~1.0 is found, corresponding to a TD rotation of ~20° towards the $(1\,1\,4)[\bar{2}\,\bar{2}\,1]$ (G^T) orientation. A true strain of similar magnitude is also found in the lower Cu layer close to the interface between this layer and the upper Nb layer. However, in that region a small rotation angle of ~5° and insignificant shear banding are observed. In both, the upper and the lower Nb layers, a rotation about TD//<110> of the original Brass-R orientation of ~20° is found near the phase boundaries, leading to a texture component near (1 1 0)[0 0 1]. Also, significant shear banding accompanied by strain localization (above 2.0) occurs at those points. For the remaining bulk region of the Nb layers, both, shear banding and strain are insignificant. Accordingly, the rotation angle decreases to ~10° at the points. We observe that significant grain rotations in Nb correspond to the positions of highest strain accumulation and also coincide with the occurrence

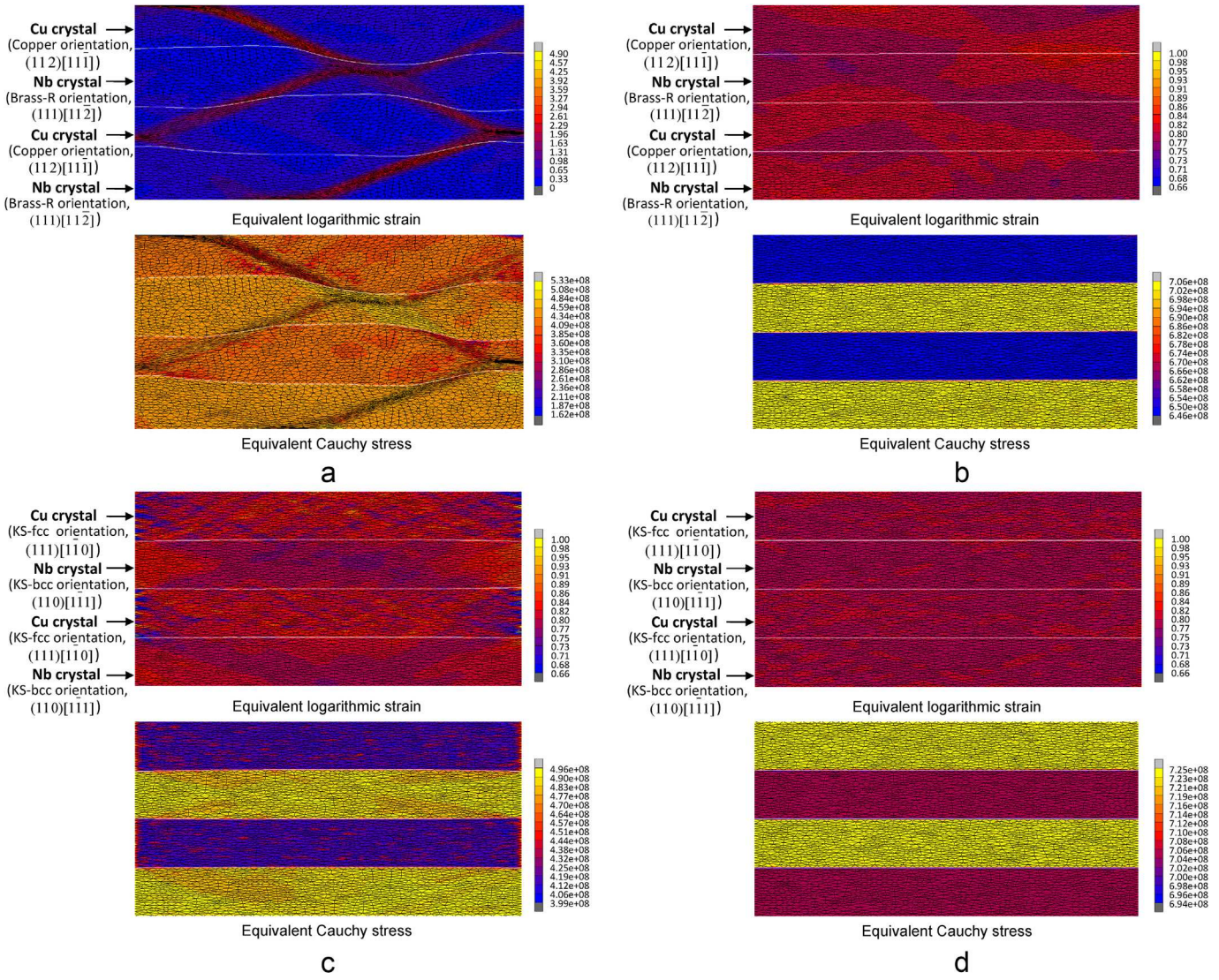

Fig. 4. Predicted distributions of equivalent logarithmic strain and equivalent Cauchy stress for Cu-Nb quadricrystals with different initial orientations and single-layer thicknesses at 50% thickness reduction: (a) Cu (Copper orientation, $(1\,1\,2)[1\,1\,\bar{1}]$) plus Nb (Brass-R orientation, $(1\,1\,1)[1\,1\,\bar{2}]$) heterophase quadricrystal with initial layer thickness of 4 μm, (b) Cu (Copper orientation, $(1\,1\,2)[1\,1\,\bar{1}]$) plus Nb (Brass-R orientation, $(1\,1\,1)[1\,1\,\bar{2}]$) heterophase quadricrystal with initial layer thickness of 75 nm, (c) Cu (KS-fcc orientation, $(1\,1\,1)[1\,\bar{1}\,0]$) plus Nb (KS-bcc orientation, $(1\,1\,0)[1\,\bar{1}\,1]$) heterophase quadricrystal with initial layer thickness of 4 μm and (d) Cu (KS-fcc orientation, $(1\,1\,1)[1\,\bar{1}\,0]$) plus Nb (KS-bcc orientation, $(1\,1\,0)[1\,\bar{1}\,1]$) heterophase quadricrystal with initial layer thickness of 75 nm.

of shear bands. This agrees with the in-band volume rotation reported in a cold rolled iron-silicon alloy with bcc crystal structure [63]. Therefore, in both phases larger rotations (above 10°) are closely related to the occurrence of shear bands.

For the Cu (KS-fcc orientation) plus Nb (KS-bcc orientation) quadricrystal, the rotation angle in the Cu layers is within the range of 10–25° (Fig. 5b). This corresponds to the rotation about both ND and TD axes from the original orientation towards the $(1\,1\,2)[1\,1\,\bar{1}]$ texture component. Inhomogeneous distribution of shear bands is also found within this phase. Therefore, the grain rotations as well as some strain localization in Cu are induced by dislocation slip and shear banding. In addition, a smaller maximum rotation angle is found in the Cu layers compared with Cu single crystal, which is attributed to the weak shear banding of the former (Fig. 3b). The initial KS-bcc orientation of the Nb layers is advantageous for initiating shear banding. Accordingly, a uniform shear banding-related microstructure evolves in this phase. This contributes to the generally homogeneous strain distribution (~0.8) and grain rotation about the TD axis. Also, a rotation of the Nb layer about ED that coincides with dislocation slip is observed. These two rotations jointly lead to a texture component close to $(1\,1\,1)[1\,2\,\bar{3}]$.

4.2. Micromechanical behavior as a function of initial layer thickness

As demonstrated above, the initiation of shear banding in multiphase laminates depends on the inherent phase properties and their orientations. According to the simulations for quadricrystals with layer thickness ranging from 35 μm to 75 nm, the shear banding behavior of each metal is found to be also influenced by the initial layer thickness. The evolution of the normalized shear rates on the twinning and shear band systems for individual phases in the studied quadricrystals is presented in Fig. 6. The results indicate quite different micromechanical behavior of the same orientations embedded in micrometer- and in nanometer-scaled microstructures. For the Cu (Copper orientation) plus Nb (Brass-R

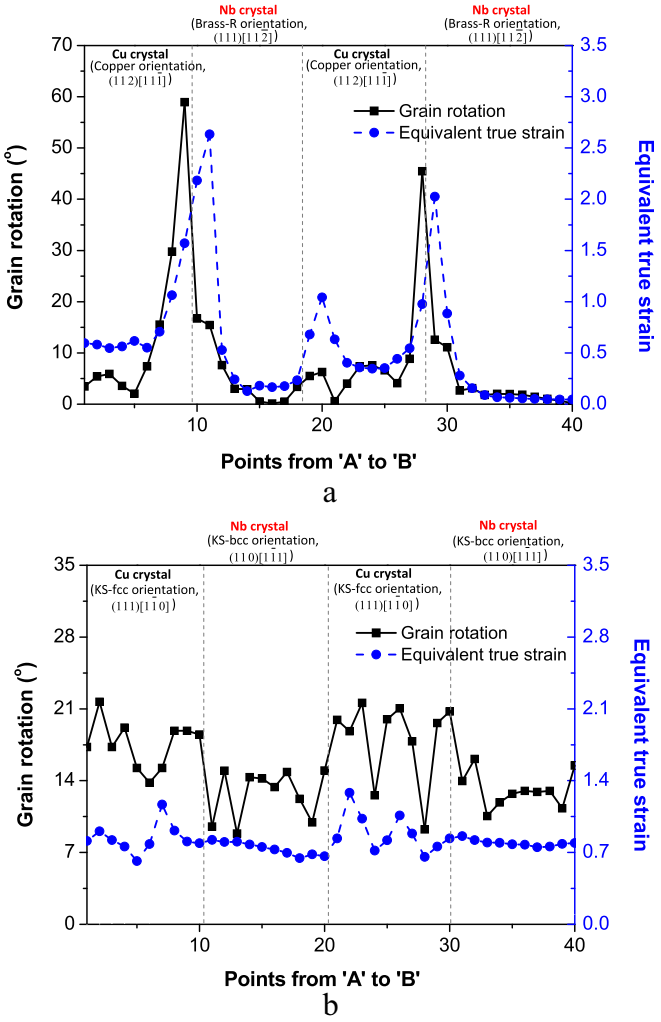

Fig. 5. Predicted evolution of grain rotation angle with respect to its original orientation and equivalent true strain for each phase in 50% deformed Cu-Nb quadricrystals with an initial layer thickness of 35 μm, along the line scan from 'A' to 'B' (as marked in Fig. 3) for the corresponding models: (a) Cu (Copper orientation, (1 1 2)[1 1 $\bar{1}$]) plus Nb (Brass-R orientation, (1 1 1)[1 1 $\bar{2}$]) heterophase quadricrystal and (b) Cu (KS-fcc orientation, (1 1 1)[1 $\bar{1}$ 0]) plus Nb (KS-bcc orientation, (1 1 0)[1 $\bar{1}$ 1]) heterophase quadricrystal. On each line the grain rotation angle and equivalent true strain at 40 evenly distributed points are evaluated.

orientation) quadricrystals with initial single layer thicknesses of 35 μm and 4 μm (Fig. 6a and b), the Cu and Nb layers show an increasing contribution of both shear banding and twinning to the overall deformation at around 5% thickness reduction (0.05 strain). However, for the quadricrystal with an initial single layer thickness of 75 nm, pronounced activation of shear bands occurs at an early stage of plastic deformation, and with further straining shear banding prevails over the other deformation mechanisms. In this quadricrystal, the magnitude of the shear band contribution is much larger than that in the micrometer-scaled cases. In addition, much less contribution from twinning is predicted for the Cu layers, which agrees with the experimental observation that twinning does not occur in 50% rolled Cu-Nb thin films with 75 nm starting layer thickness [2] or roll-bonded Cu-Nb composites with average layer thickness of 200 nm [64]. For the Cu (KS-fcc orientation) plus Nb (KS-bcc orientation) quadricrystal, the magnitude of the shear band contribution to deformation also varies among the different microstructures in both phases. More specifically, the contribution of shear banding proceeds in the order: 75 nm, 4 μm, 35 μm. Moreover, at ~50% thickness reduction (0.693 strain) the contribution from shear banding increases as the initial single layer thickness becomes finer (Fig. 6c and d).

To this stage, the length-scale dependent mechanical behavior of the rolled Cu-Nb quadricrystals as a function of initial single layer thickness can be summarized below. For the multilayers with an initial single layer thickness of 35 μm or 4 μm, the layer thickness reduction is non-uniform. The curved Cu/Nb interface indicates the heterogeneity in deformation. Rolling textures typically found in fcc and bcc metals are developed in the Cu and Nb layers, respectively. These results are consistent with the experimental observation that a high density of dislocations/cell structures form in the Cu-Nb multilayers with initial single layer thicknesses of micrometer scale [4]. For the nanometer-scaled multilayers, completely different behavior is predicted: Both, the Cu and the Nb layers reduce uniformly in thickness and the initial orientation relations are preserved. These features have also been verified by experimental studies on a Cu-Nb multilayered film with an initial single layer thickness of 75 nm where only insignificant changes in dislocation density occur within the layers even after 50% thickness reduction [4,65]. At the length scale of micrometers, the modeling for the Cu-Nb quadricrystals has shown that dislocation slip is the dominant deformation mechanism, even though shear banding increasingly carries the deformation at the late stage of straining. Besides shear banding the heterogeneity of deformation can be attributed to the dislocation pile-up mechanism. As the mean free path of the dislocations becomes significantly lower than the layer thickness, dislocation networks that induce plastic shear concentration at the interfaces between the layers are formed. Moreover, because of the stochastic nature of the dislocation sources [4], the layer thickness within the multilayered structure is reduced non-uniformly with deformation. At a layer thickness of 75 nm, however, the dislocation source to obstacle distance is limited, preventing dislocation pile up at the heterophase interfaces.

As most of the experimental studies on deformed Cu-Nb composites are available for multilayers with an interface plane $<111>_{Cu}/<110>_{Nb}$, we focus in the following discussion on composites with an initial K-S orientation relation between the two phases. Simulation of the micrometer-sized Cu (KS-fcc orientation) plus Nb (KS-bcc orientation) quadricrystal has shown that at the initial stage of plastic deformation, compression perpendicular to the {110} plane induces homogeneous slip on four slip systems in the Nb phase, i.e. (0 1 1)[$\bar{1}$ $\bar{1}$ 1], (1 0 1)[$\bar{1}$ $\bar{1}$ 1], (0 $\bar{1}$ 1)[1 1 1] and (1 0 $\bar{1}$)[1 1 1], which prevents local rotation of the grain. This behavior agrees with the theoretical analysis that on these symmetrically activated slip systems the resolved shear stress is equal [2]. With increasing strain, the simulation shows that the non-crystallographic shear contribution, i.e. shear banding, increases and starts to prevail over dislocation shear at around 0.2 strain. The principal stresses governing the constitutive shear band law are derived by principal axis transformation from the second Piola-Krichoff stress tensor. Ordering these principal stresses according to $|\sigma_1| \geq |\sigma_2| \geq |\sigma_3|$ with $\sigma_1 \leq 0$, $\sigma_2 \leq 0$, $\sigma_3 \geq 0$ (cf. Eq. (13)) reveals that the shear stress in the plane constructed by the two orthonormal principal directions $\hat{\mathbf{e}}_1$ and $\hat{\mathbf{e}}_3$ (corresponding to the maximum compression stress and the tensile stress) is promoting shear banding. In a shear band system χ the rotation increment around the $-i \times j$ axis is calculated as

$$\dot{\omega}_{ij}^{\chi} = 0.5\dot{\gamma}^{\chi}\left(m_j n_i - m_i n_j\right)^{\chi} \tag{17}$$

with i and j being Cartesian indices, and m and n the direction and plane normal of the shear band system. A net rotation of zero is then induced by deformation on the two symmetrically activated

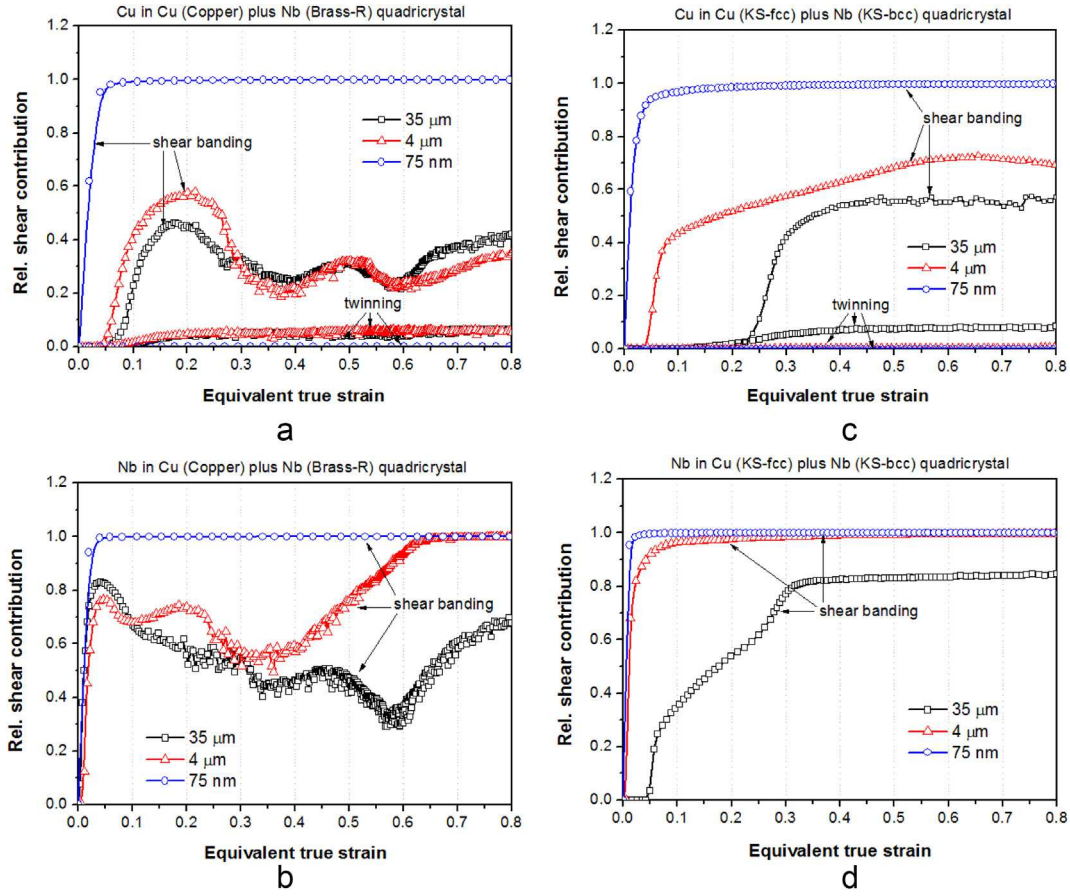

Fig. 6. Predicted relative shear contributed by the different deformation mechanisms (twinning and non-crystallographic shear banding) as a function of the equivalent true strain for (a) Cu and (b) Nb crystals in the Cu (Copper orientation) plus Nb (Brass-R orientation) quadricrystal, and (c) Cu and (d) Nb crystals in the Cu (KS-fcc orientation) plus Nb (KS-bcc orientation) quadricrystal with different initial layer thickness during plane strain compression. As the total shear contribution from dislocation slip, twinning and shear banding for an individual crystal is 1.0, the relative shear from dislocation slip is not shown.

$(\hat{\mathbf{e}}_1 - \hat{\mathbf{e}}_3)$-shear band planes. In addition, the stress field in the shear band region triggers the activation of some other slip systems that are not preferentially activated at small deformations because of their low Schmid factor. The modeling shows that when shear banding has been extensively activated within the Nb layers, dislocation slip on a pair of co-planar systems $(1\,\bar{1}\,2)[\bar{1}\,1\,1]$ and $(1\,\bar{1}\,2)[1\,1\,1]$ starts to take place in the shear band region. This altered dislocation activity leads to additional grain rotation around both TD and ED towards the {111} components. A consistent result is also found for the Cu layers with the compression axis perpendicular to the {111} plane, showing the activation of new slip systems in the strain localized region. More specific, the initial deformation mainly proceeds on the $(\bar{1}\,\bar{1}\,1)[0\,\bar{1}\,\bar{1}]$ and $(\bar{1}\,\bar{1}\,1)[1\,0\,1]$ pair of co-planar systems together with the $(1\,\bar{1}\,\bar{1})[\bar{1}\,0\,\bar{1}]$ and $(\bar{1}\,1\,\bar{1})[0\,1\,1]$ slip systems. At a strain above ~0.2 where dislocation slip on the above-mentioned systems sharply drops, the shear rate on the shear band systems increases with deformation. In addition, accompanied by the activation of shear banding, some other slip systems, i.e. $(1\,1\,1)[1\,\bar{1}\,0]$, $(1\,\bar{1}\,\bar{1})[1\,1\,0]$ and $(\bar{1}\,1\,\bar{1})[\bar{1}\,\bar{1}\,0]$, become more active. These systems also operate within the shear bands, implying an increase of the local Schmid factor under the stress field which is modulated by the shear banding. One should note that the equal activation of the symmetric shear band systems does not cause grain rotation itself, thus the significant orientation transition from the initial component to a rolling texture for the micrometer-scaled Cu layers is attributed to the activation of the new slip systems.

For better demonstrating the effects of different micro-mechanisms on the texture development of multilayered Cu-Nb composites, Fig. 7 shows the $\varphi_2 = 45°$ODF sections from Cu and Nb of the 50% rolled samples with the initial single layer thicknesses of 4 μm and 75 nm, respectively. The ODF sections obtained from X-ray diffraction [1] are also presented for comparison. As the experimental composites do not show alignment of the in-plane K-S relation, i.e. $<110>_{Cu}//<111>_{Nb}$, between adjacent Cu and Nb column grain pairs in the as-deposited condition, the simulations here apply the $<111>_{Cu}$ and $<110>_{Nb}$ fibers that fulfill the out-of-plane K-S relation as the initial textures of the individual phases. Both, experiments and simulations show that the textures developed in the 4 μm initial single layer thickness composite consist of typical fcc rolling components for Cu (including Copper, Goss and Brass orientations), and partial α fiber and γ fiber bcc texture components (including $(1\,1\,2)[1\,\bar{1}\,0]$, $(1\,1\,1)[1\,\bar{1}\,0]$ and $(1\,1\,1)[1\,1\,\bar{2}]$ orientations) for Nb, respectively. For the rolled 75 nm initial single layer thickness composite, different textures are obtained by both, experiment and modeling. There is only little rotation around ED and the K-S orientation relation is generally preserved during deformation. Earlier work [1,2] suggests that for nanometer-scaled composites after large strains the preservation of interface crystallography is due to activation of symmetric slip. However, the current simulation clearly shows that the activation of the non-crystallographic shear band systems determined by the transient stress field has been prevailing in the respective phases since an early stage of plastic deformation. This agrees well with

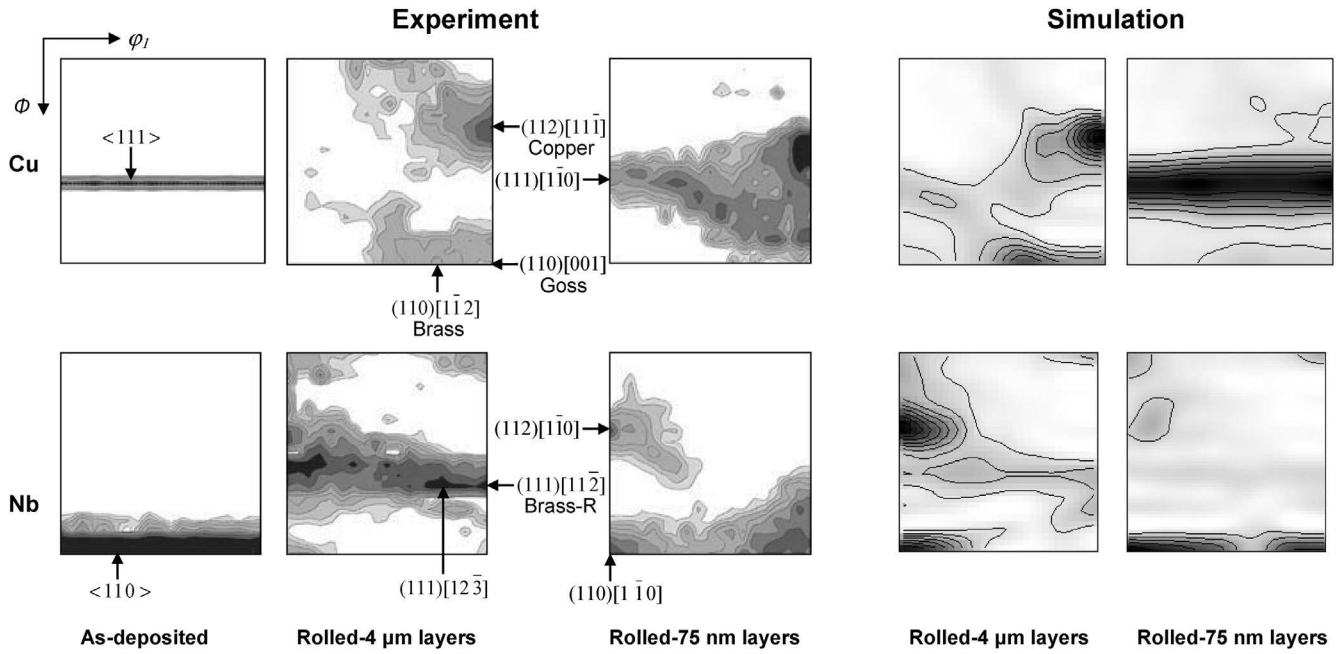

Fig. 7. Experimental and simulated ODF sections with constant $\varphi_2 = 45°$ for Cu and Nb in the multilayered composites at the as-deposited state and after deformation to 50% thickness reduction. The results for the composites with initial layer thicknesses of 4 μm and 75 nm are presented, respectively. The experimental data is obtained from Ref. [1]. Orientation density levels: 1.0, 2.0, …, 8.0.

the experimental observation that through-thickness shear bands often form in cold rolled heterophase nanolaminates [4–7,22–25,61]. Specially, fracture of such materials often occurs through shear cracks and the crack plane roughly along the plane with maximum shear stress is inclined towards ED. It is also worth noting that, compared with micrometer-scaled multilayers, the structure with initial single layer thickness of a few tens of nanometers possesses much less spacing for dislocation slip, suppressing multiplication of dislocations inside the layer. Also, in the nanostructured confined state the length of partial dislocations required for forming a twin nucleus becomes limited [66]. Then, the correlated bow-out of three partial dislocations as required for a twin nucleation event [49] may not occur sufficiently. These points explain the suppression of dislocation slip and twinning and the associated prevalence of shear banding in nanometer-scaled composites. Therefore, as revealed by the current simulations, these deformation features lead to completely different deformation textures for multilayers with micrometer or nanometer initial length scales.

5. Conclusions

We have presented CPFE simulations on the deformation microstructures, plastic flow and crystallographic texture evolution in multilayered Cu-Nb composites during cold rolling. To study the underlying micromechanics of the composites, characteristic initial orientation combinations and layer thicknesses are considered in a series of quadricrystal simulations. The main results are:

(1) In composite materials, significant non-crystallographic shear banding may occur in both fcc and bcc phases, primarily determined by their specific initial orientations. For an individual phase within the composites, the activation of shear banding is also determined by the mechanical properties and orientations of its adjacent phase. At the heterophase interfaces, where stress concentrations occur, pronounced shear banding can be triggered so as to accommodate plastic deformation between the adjacent phases.

(2) For multilayered composites with an initial layer thickness of 35 μm or 4 μm, respectively, the layer thickness reduction after cold rolling is non-uniform. The distorted heterophase interface indicates the heterogeneity in the overall co-deformation field. The rolling textures which are typically found in fcc and bcc metals are developed in the Cu and Nb layers inside the composite, respectively. For the 75 nm layer thickness composite, both, the Cu and Nb layers are reduced more uniformly in thickness and the initial orientations are preserved in the respective layers after deformation. These features match corresponding experimental observations made on cold-rolled Cu-Nb thin films with different initial single layer thicknesses.

(3) The simulations reveal that for composites with an initial single layer thickness of micrometer scale dislocation slip is the dominant deformation mechanism, even though shear banding increasingly carries the deformation at the late stages of straining. For samples with an initial single layer thickness of only a few tens of nanometers, however, shear banding together with limited dislocation slip prevails as deformation mechanism. The more diffuse nature of non-crystallographic shear banding, i.e. the homogeneous distribution of shear bands within microstructures, leads to the homogeneous deformation of the nanometer-scaled composites. The slip activity which is adjusted by shear banding leads to different deformation textures in the small scaled multilayers compared to materials with coarser initial microstructure dimensions.

Acknowledgments

This work was financially supported by the National Natural Science Foundation of China (No. 51571057), the Program for New Century Excellent Talents in University (No. NCET-13-0104) and the

joint open fund supported by Liaoning Natural Science Foundation and Shenyang National Laboratory for Materials Science (No. 2015021003).

Appendix A. Supplementary data

Supplementary data related to this article can be found at http://dx.doi.org/10.1016/j.actamat.2016.03.055.

References

[1] P.M. Anderson, J.F. Bingert, A. Misra, J.P. Hirth, Rolling textures in nanoscale Cu/Nb multilayers, Acta Mater 51 (2003) 6059–6075.
[2] A. Misra, J.P. Hirth, R.G. Hoagland, J.D. Embury, H. Kung, Dislocation mechanisms and symmetric slip in rolled nano-scale metallic multilayers, Acta Mater 52 (2004) 2387–2394.
[3] A. Misra, J.P. Hirth, R.G. Hoagland, Length-scale-dependent deformation mechanisms in incoherent metallic multilayered composites, Acta Mater 53 (2005) 4817–4824.
[4] A. Misra, R.G. Hoagland, Plastic flow stability of metallic nanolaminate composites, J. Mater. Sci. 42 (2007) 1765–1771.
[5] Y.P. Li, J. Tan, G.P. Zhang, Interface instability within shear bands in nanoscale Au/Cu multilayers, Scr. Mater 59 (2008) 1226–1229.
[6] Y.P. Li, G.P. Zhang, On plasticity and fracture of nanostructured Cu/X (X=Au, Cr) multilayers: The effects of length scale and interface/boundary, Acta Mater 58 (2010) 3877–3887.
[7] J.Y. Zhang, Y. Liu, J. Chen, Y. Chen, G. Liu, X. Zhang, J. Sun, Mechanical properties of crystalline Cu/Zr and crystal–amorphous Cu/Cu–Zr multilayers, Mater. Sci. Eng. A 552 (2012) 392–398.
[8] S. Zheng, I.J. Beyerlein, J.S. Carpenter, K. Kang, J. Wang, W. Han, N.A. Mara, High-strength and thermally stable bulk nanolayered composites due to twin-induced interfaces, Nat. Commun. 4 (2013) 1696.
[9] W.Z. Han, M.J. Demkowicz, N.A. Mara, E.G. Fu, S. Sinha, A.D. Rollett, Y.Q. Wang, J.S. Carpenter, I.J. Beyerlein, A. Misra, Design of radiation tolerant materials via interface engineering, Adv. Mater 25 (2013) 6975–6979.
[10] J.Y. Zhang, J. Li, X.Q. Liang, G. Liu, J. Sun, Achieving optimum mechanical performance in metallic nanolayered Cu/X (X=Zr, Cr) micropillars, Sci. Rep. 4 (2014) 4205.
[11] W.Z. Han, E.K. Cerreta, N.A. Mara, I.J. Beyerlein, J.S. Carpenter, S.J. Zheng, C.P. Trujillo, P.O. Dickerson, A. Misra, Deformation and failure of shocked bulk Cu–Nb nanolaminates, Acta Mater 63 (2014) 150–161.
[12] D. Raabe, U. Hangen, Correlation of microstructure and type II superconductivity of a heavily cold rolled Cu-20mass% Nb in situ composite, Acta Mater 44 (1996) 953–961.
[13] U. Hangen, D. Raabe, Experimental investigation and simulation of the normal conducting properties of a heavily cold rolled Cu-20 mass%Nb in situ composite, Phys. Status. Solid 147 (1995) 515–527.
[14] D. Raabe, F. Heringhaus, Correlation of superconductivity and microstructure in an in-situ formed Cu-20%Nb composite, Phys. Status. Solid 142 (1994) 473–481.
[15] D. Raabe, U. Hangen, On the anisotropy of the superconducting properties of a heavily cold rolled cu-20 mass% Nb in situ composite, Phys. Status. Solid 154 (1996) 715–726.
[16] U. Hangen, D. Raabe, Modelling of the yield strength of a heavily wire drawn Cu-20%Nb composite by use of a modified linear rule of mixtures, Acta Metall. Mater 43 (1995) 4075–4082.
[17] J.D. Embury, J.P. Hirth, On dislocation storage and the mechanical response of fine scale microstructures, Acta Metall. Mater 42 (1994) 2051–2056.
[18] M.A. Phillips, B.M. Clemens, W.D. Nix, A model for dislocation behavior during deformation of Al/Al3Sc (fcc/L12) metallic multilayers, Acta Mater 51 (2003) 3157–3170.
[19] D. Raabe, P.-P. Choi, Y. Li, A. Kostka, X. Sauvage, F. Lecouturier, K. Hono, R. Kirchheim, R. Pippan, D. Embury, Metallic composites processed via extreme deformation: Toward the limits of strength in bulk materials, MRS Bull. 35 (2010) 982–991.
[20] W. Guo, E.A. Jägle, P.-P. Choi, J. Yao, A. Kostka, J.M. Schneider, D. Raabe, Shear-induced mixing governs codeformation of crystalline-amorphous nanolaminates, Phys. Rev. Lett. 113 (2014) 035501.
[21] Y. Li, D. Raabe, M. Herbig, P.-P. Choi, S. Goto, A. Kostka, H. Yarita, C. Borchers, R. Kirchheim, Segregation stabilizes nanocrystalline bulk steel with near theoretical strength, Phys. Rev. Lett. 113 (2014) 106104.
[22] S. Ohsaki, S. Kato, N. Tsuji, T. Ohkubo, K. Hono, Bulk mechanical alloying of Cu–Ag and Cu/Zr two-phase microstructures by accumulative roll-bonding process, Acta Mater 55 (2007) 2885–2895.
[23] C.A. Davy, K. Han, P.N. Kalu, S.T. Bole, Supercond, 2008;18:560.Examinations of Cu-Ag composite conductors in sheet forms, IEEE Trans. Appl. Supercond. 18 (2008) 560–563.
[24] D. Raabe, F. Heringhaus, U. Hangen, G. Gottstein, Investigation of a Cu-20 mass % Nb in situ composite Part I: fabrication, microstructure and mechanical properties, Z. Met. 86 (1995) 405–415.
[25] X. Sauvage, L. Renaud, B. Deconihout, D. Blavette, D.H. Ping, K. Hono, Solid state amorphization in cold drawn Cu/Nb wires, Acta Mater 49 (2001) 389–394.
[26] H. Sheikh, Role of shear banding on the microtexture of an Al-Mg alloy processed by hot/high strain rate accumulative roll bonding, Scr. Mater 64 (2011) 556–559.
[27] M. Knezevic, T. Nizolek, M. Ardeljan, I.J. Beyerlein, N.A. Mara, T.M. Pollock, Texture evolution in two-phase Zr/Nb lamellar composites during accumulative roll bonding, Int. J. Plast. 57 (2014) 16–28.
[28] M. Ardeljan, M. Knezevic, T. Nizolek, I.J. Beyerlein, N.A. Mara, T.M. Pollock, A study of microstructure-driven strain localizations in two-phase polycrystalline HCP/BCC composites using a multi-scale model, Int. J. Plast. 74 (2015) 35–57.
[29] J. Hirsch, K. Lücke, Mechanism of deformation and development of rolling textures in polycrystalline f.c.c. metals—I. Desprication of rolling texture development in homogeneous CuZn alloys, Acta Metall. 36 (1988) 2863–2882.
[30] H. Paul, J.H. Driver, C. Maurice, Z. Jasieński, Shear band microtexture formation in twinned face centred cubic single crystals, Mater. Sci. Eng. A 359 (2003) 178–191.
[31] H. Paul, A. Morawiec, J.H. Driver, E. Bouzy, On twinning and shear banding in a Cu-8 at.% Al alloy plane strain compressed at 77 K, Int. J. Plast. 25 (2009) 1588–1608.
[32] C.S. Hong, N.R. Tao, X. Huang, K. Lu, Nucleation and thickening of shear bands in nano-scale twin/matrix lamellae of a Cu–Al alloy processed by dynamic plastic deformation, Acta Mater 58 (2010) 3103–3116.
[33] F.K. Yan, N.R. Tao, F. Archie, I. Gutierrez-Urrutia, D. Raabe, K. Lu, Deformation mechanisms in an austenitic single-phase duplex microstructured steel with nanotwinned grains, Acta Mater 81 (2014) 487–500.
[34] N.V. Govindaraj, J.G. Frydendahl, B. Holmedal, Layer continuity in accumulative roll bonding of dissimilar material combinations, Mate. Des. 52 (2013) 905–915.
[35] F. Heringhaus, D. Raabe, U. Hangen, G. Gottstein, Textures of rolled and wire drawn Cu-20%Nb, Mater. Sci. Forum 157–162 (1994) 709–714.
[36] D. Raabe, K. Lücke, Rolling textures of niobium and molybdenum, Z. Met. 85 (1994) 302–306.
[37] D. Raabe, J. Ball, G. Gottstein, Rolling textures of a Cu-20%Nb composite, Scr. Metall. Mater 27 (1992) 211–216.
[38] H.R.Z. Sandim, D. Raabe, EBSD study of grain subdivision of a Goss grain in coarse-grained cold-rolled niobium, Scr. Mater 53 (2005) 207–212.
[39] J.S. Carpenter, S.C. Vogel, J.E. LeDonne, D.L. Hammon, I.J. Beyerlein, N.A. Mara, Bulk texture evolution of Cu–Nb nanolamellar composites during accumulative roll bonding, Acta Mater 60 (2012) 1576–1586.
[40] I.J. Beyerlein, N.A. Mara, D. Bhattacharyya, D.J. Alexander, C.T. Necker, Texture evolution via combined slip and deformation twinning in rolled silver–copper cast eutectic nanocomposite, Int. J. Plast. 27 (2011) 121–146.
[41] N. Jia, D. Raabe, X. Zhao, Texture and microstructure evolution during non-crystallographic shear banding in a plane strain compressed Cu–Ag metal matrix composite, Acta Mater 76 (2014) 238–251.
[42] J.S. Carpenter, T. Nizolek, R.J. McCabe, M. Knezevic, S.J. Zheng, B.P. Eftink, J.E. Scott, S.C. Vogel, T.M. Pollock, N.A. Mara, I.J. Beyerlein, Bulk texture evolution of nanolamellar Zr–Nb composites processed via accumulative roll bonding, Acta Mater 92 (2015) 97–108.
[43] N. Jia, F. Roters, P. Eisenlohr, C. Kords, D. Raabe, Non-crystallographic shear banding in crystal plasticity FEM simulations: Example of texture evolution in α-brass, Acta Mater 60 (2012) 1099–1115.
[44] S.R. Kalidindi, Modeling anisotropic strain hardening and deformation textures in low stacking fault energy fcc metals, Int. J. Plast. 17 (2001) 837–860.
[45] D.R. Steinmetz, T. Jäpel, B. Wietbrock, P. Eisenlohr, I. Gutierrez-Urrutia, A. Saeed-Akbari, T. Hickel, F. Roters, D. Raabe, Revealing the strain-hardening behavior of twinning-induced plasticity steels: theory, simulations, experiments, Acta Mater 61 (2013) 494–510.
[46] W. Blum, P. Eisenlohr, Dislocation mechanics of creep, Mater. Sci. Eng. A 510–511 (2009) 7–13.
[47] F. Roters, Advanced Material Models for the Crystal Plasticity Finite Element Method: Development of a General CPFEM Framework, Habilitation thesis, RWTH Aachen, Germany, 2011.
[48] A. Ma, F. Roters, A constitutive model for fcc single crystals based on dislocation densities and its application to uniaxial compression of aluminium single crystals, Acta Mater 52 (2004) 3603–3612.
[49] S. Mahajan, G.Y. Chin, Formation of deformation twins in f.c.c. crystals, Acta Metall. 21 (1973) 1353–1363.
[50] L. Anand, C. Su, A theory for amorphous viscoplastic materials undergoing finite deformations, with application to metallic glasses, J. Mech. Phys. Solids 53 (2005) 1362–1396.
[51] D. Kuhlmann-Wilsdorf, H. Wilsdorf, The surface structures of deformed aluminium, copper, silver and alpha-brass and their theoretical interpretation, Acta Metall. 1 (1953) 394–399.
[52] S. Nemat-Nasser, W.G. Guo, Flow stress of commercially pure niobium over a broad range of temperatures and strain rates, Mater. Sci. Eng. A 284 (2000) 202–210.
[53] D. Raabe, Taylor simulation and experimental investigation of rolling textures of polycrystalline iron aluminides with special regard to slip on {112} planes, Acta Mater 44 (1996) 937–951.
[54] D. Raabe, Investigation of contribution of {123} slip planes to development of rolling textures in bee metals by use of Taylor models, Mater. Sci. Tech. 11

(1995) 455–460.
[55] J.S. Carpenter, R.J. McCabe, I.J. Beyerlein, T.A. Wynn, N.A. Mara, A wedge-mounting technique for nanoscale electron backscatter diffraction, J. Appl. Phys. 113 (2013) 094304.
[56] F. Roters, P. Eisenlohr, L. Hantcherli, D.D. Tjahjanto, T.R. Bieler, D. Raabe, Overview of constitutive laws, kinematics, homogenization and multiscale methods in crystal plasticity finite-element modeling: theory, experiments, applications, Acta Mater 58 (2010) 1152–1211.
[57] F. Roters, P. Eisenlohr, C. Kords, D.D. Tjahjanto, M. Diehl, D. Raabe, DAMASK: the Düsseldorf advanced material simulation kit for studying crystal plasticity using an FE based or a spectral numerical solver, Proc. IUTAM 3 (2012) 3–10.
[58] M. Sachtleber, Z. Zhao, D. Raabe, Experimental investigation of plastic grain interaction, Mater. sci.eng. A 336 (2002) 81–87.
[59] N. Jia, F. Roters, P. Eisenlohr, D. Raabe, X. Zhao, Simulation of shear banding in heterophase co-deformation: example of plane strain compressed Cu–Ag and Cu–Nb metal matrix composites, Acta Mater 61 (2013) 4591–4606.
[60] M. Kuroda, V. Tvergaard, Effects of texture on shear band formation in plane strain tension/compression and bending, Int. J. Plast. 23 (2007) 244–272.
[61] D. Raabe, S. Ohsaki, K. Hono, Mechanical alloying and amorphization in Cu-Nb-Ag in situ composite wires studied by transmission electron microscopy and atom probe tomography, Acta Mater 57 (2009) 5254–5263.
[62] N. Jia, P. Eisenlohr, F. Roters, D. Raabe, X. Zhao, Orientation dependence of shear banding in face-centered-cubic single crystals, Acta Mater 60 (2012) 3415–3434.
[63] T. Nguyen-Minh, J.J. Sidor, R.H. Petrov, L.A.I. Kestens, Occurrence of shear bands in rotated Goss ({110}<110>) orientations of metals with bcc crystal structure, Scr. Mater 67 (2012) 935–938.
[64] S.C.V. Lim, A.D. Rollett, Length scale effects on recrystallization and texture evolution in Cu layers of a roll-bonded Cu–Nb composite, Mater. Sci. Eng. A 520 (2009) 189–196.
[65] K. Nyilas, A. Misra, T. Ungár, Micro-strains in cold rolled Cu–Nb nanolayered composites determined by X-ray line profile analysis, Acta Mater 54 (2006) 751–755.
[66] Y.F. Shen, N. Jia, Y.D. Wang, X. Sun, L. Zuo, D. Raabe, Suppression of twinning and phase transformation in an ultrafine grained 2 GPa strong metastable austenitic steel: Experiment and simulation, Acta Mater 97 (2015) 305–315.